Quantifying the impact of fire events on dust emission potential from partially vegetated dunes in the southwest Kalahari

Abstract

The removal of stabilising vegetation from sand dunes by fire has been widely linked to increases in aeolian sediment transport and dune movement. However, substantial gaps exist in our knowledge of whether burned dunes in arid environments have the potential to emit dust. To explore relationships between fire and dust emission on partially vegetated sand dunes in the Namibian Kalahari Desert, 180 measurements of wind erosion threshold and dust flux were carried out using a portable wind tunnel (Portable In-Situ Wind Erosion Laboratory or PI-SWERL). Data were analysed to compare erosion thresholds and dust emission flux on adjacent burned and unburned sites. The data suggest that both burned and unburned dune crests, flanks, and interdunes have a low potential for dust emission. Whilst there was no significant difference in dust emission flux between burned and unburned control surfaces (Kruskal-Wallis, $p > 0.05$), there was evidence of significantly higher erosion thresholds on burned surfaces (T-test, $p < 0.01$). Where the surface had been disturbed, resulting in the removal of the typically present biological soil crusts (biocrust), our data suggest that dust emission fluxes are, on average, 8-13 times higher those of undisturbed surfaces. The analysis reveals that even when burned and devoid of vegetation, the Kalahari linear dune system is sediment-availability limited. This finding indicates the importance of ground surface characteristics, such as biocrusts, in preventing dust emission from the Kalahari dune field.

Key words: Dust; Fire; Kalahari; PI-SWERL; Sand dunes

Highlights:

- Experimental results from the first wind tunnel study of burned dunes are presented
- Fire does not have a significant intensifying effect on dust emission
- Threshold shear velocities increased on burned areas compared to unburned surfaces
- Surfaces where biological soil crusts had been removed produced large dust fluxes

1. Introduction

Accurately quantifying mineral dust emissions from diverse landscapes is crucial for understanding atmospheric dust loading and its climatic and environmental impacts (Schepanski, 2018; Field et al., 2010; Kok et al., 2023; Gill, 2018). However, current atmospheric models are not in agreement on the sources and emission flux of existing atmospheric dust (Kok et al., 2021b; Chappell et al., 2023; Mahowald et al., 2024; Kim et al., 2024). Models rely on field studies to quantify surface controls on emissions and satellite data to estimate the amount of dust in the atmosphere (Webb and Strong, 2011; Haustein et al., 2015; Klose et al., 2019). There are several uncertainties in the data on dust flux and source locations used in the atmospheric models including: low-resolution remote sensing imagery often fails to detect emission sources (Urban et al., 2018; von Holdt et al., 2019); challenges in characterising surface properties of key emission sources (Webb and Strong, 2011); and the miscalculation of coarse dust in the atmosphere (Adebiyi et al., 2023). Another key uncertainty in dust and atmospheric modelling is the accurate quantification of low-concentration or infrequent emission dust sources, which are difficult to capture due to their irregularity and the limitations of remote sensing technologies (Urban et al., 2018; Sweeney et al., 2023; Wagenbrenner et al., 2017; Okin et al., 2011).

The entrainment of dust from the Earth's surface is a complex interaction of factors that influence the erosivity of the wind and/or the erodibility of the surface (Webb et al., 2021; Wiggs et al., 2022). For dust particles to be entrained, wind speed must exceed a critical shear velocity threshold, though this threshold is influenced by

numerous surface characteristics (Kok et al., 2012; Reynolds et al., 2007; Field et al., 2010; von Holdt et al., 2019). These characteristics are highly variable in time and space and include sediment size, surface moisture, presence of a surface crust (both biological and physical), particle abrasion, surface roughness, agglomeration of soil grains, surface geochemistry, and vegetation cover (Dickey et al., 2023; Sweeney et al., 2011; Langston and McKenna Neuman, 2005; Engelstaedter et al., 2003; Nield et al., 2011). Particle size is especially important in dust emission, as it dictates both the force required for entrainment and the potential distance particles can travel (Kok et al., 2012). Consequently, low-lying landforms filled with fine sediment, such as paleolake basins and ephemeral river or lake beds, represent some of the largest dust sources globally (Prospero et al., 2002; Bullard et al., 2011; Ginoux et al., 2012; Parajuli and Zender, 2017).

Sand dunes are not typically considered to be significant sources of atmospheric dust as they generally contain less than 5 % silt and clay (Prospero et al., 2002). Vegetated dunes are often excluded from dust emission studies because plants act to stabilise the surface, preventing sediment movement and abrasive interactions. Plant architecture increases surface roughness and provides physical sheltering, but also traps allochthonous dust particles and allows a finer fraction of sediment to build up (Suter-Burri et al., 2013; Gonzales et al., 2018). However, there is evidence to suggest that such stabilised dunes can yield larger fluxes of dust in comparison to active dunes where the surfaces have suffered recent disturbance (such as grazing, drought, or fire; Bullard et al, 2011; Sweeney et al., 2023).

It has been hypothesised that if vegetated dunes were to lose their vegetation cover and become more geomorphologically dynamic (e.g., Wiggs et al., 1995), they could potentially become large sources of dust into the future (Sweeney et al., 2023; Bhattachan et al., 2012, 2022; Pye, 1989). One of the key mechanisms by which vegetated desert dunes may become denuded of vegetation and act as low concentration emission sources of dust over short timescales is fire (Bullard et al., 2008; McGowan and Clark, 2008; Yu and Ginoux, 2022).

Sediment in many vegetated dune systems around the globe is coated in iron oxide-rich clay which can rapidly be abraded to emit fine grains (Bullard et al., 2004; Bullard and White, 2005; Swet et al., 2019). For example, abrasion studies using sediment from the vegetated dunes of the Simpson Desert in Australia found that the iron-rich clay coating of sand grains can be rapidly abraded into smaller particles (Baddock et al., 2013; Bullard and White, 2005). The Kalahari Desert in southern Africa also contains a fine fraction within its sediment that has high concentrations of soluble iron in its fine material (< 45 µm; Bhattachan et al., 2012). The iron oxide is noteworthy as, if deposited in the marine system, it can have a significant influence on ocean productivity (Jickells et al., 2005; Bhattachan et al., 2015; Dansie et al., 2022).

Burned surfaces in other desert landscapes often exhibit higher emissivity rates due to volatilised fatty acids from vegetation, which condense onto nearby sediment and form a hydrophobic coating on grains. The coating reduces interparticle cohesion by altering the contact angle of the grains (Ravi et al., 2006; Sankey et al., 2012). In the arid shrubland of the USA, Sankey et al. (2012) found that burned surfaces emitted

three times more sediment than unburned areas. Yet, there have been no field studies investigating the emissivity of burned vegetated dune fields. To understand the complexities of the impact of fire on dune dust emissions , it is crucial to examine the fire–aeolian erosion feedback mechanisms on dune environments.

There is some evidence for post-fire dust emissions from sand dune systems. For example, Yu and Ginoux (2022) used Moderate Resolution Imaging Spectroradiometer (MODIS) data (deep blue aerosol product and burned area product) and found that at the global scale wildfires lead to enhanced dust emissions. This included dust emissions from vegetated dune systems in Australia, the Sahel, and Argentina, but there are notable gaps in emission from the southwest Kalahari linear dune system (Yu and Ginoux, 2022). Further, Bullard et al. (2008) and McGowan and Clarke (2008) used remote sensing methods to detect dust plumes originating from fire scars in the Simpson Desert in Australia. But emission potential from the southwest Kalahari dune field has been poorly constrained. The Kalahari is ecologically and geomorphologically similar to the Simpson Desert in Australia (Buckley, 1981) and burns frequently (Andela et al., 2019). The Kalahari is often suggested as being a source of dust if it were to become spontaneously de-vegetated (Bhattachan et al., 2012). Yet, no research has investigated post-fire dust emissions in the region.

This research aims to fill the knowledge gap of whether the partially vegetated dunes of the southwest Kalahari have the potential to emit dust into the atmosphere because of fire destroying their protective vegetation cover and altering surface

erodibility and emissivity. Dune surface sedimentology is examined to determine changes between burned and co-located unburned plots to establish if there is fine material typical of dust in the sediment texture. Next, the emission potential between burned and unburned plots is quantified using a portable wind tunnel. The research can be broken down into two aims which are to:

1. Establish whether the southwest Kalahari dunes have a sedimentary potential to emit dust.
2. Quantify whether burning of dune vegetation has a significant effect on dust emission.

2. Methods

2.1. Study area

The research was conducted on the vegetated linear dunes (Figure 1) in the arid southwest Kalahari in Namibia in September and October 2022. The dunes consist of unconsolidated aeolian sands of mainly quartz and feldspar (Garzanti et al., 2022). There is no statistical difference in grain sizes on the east or west flank of the dunes (Lancaster, 1986): therefore, sediments in this study were collected from either face of the dune. The dune crests are spaced 0.2 to 2 km apart with heights that range from 5 to 25 m (Thomas and Leason, 2005). In this study, a crest is the highest point of the dune, a flank is 3 - 5 m down the side from the crest of the dune, and an interdune is classed as the area where the slope of the dune has become undetectable by eye.

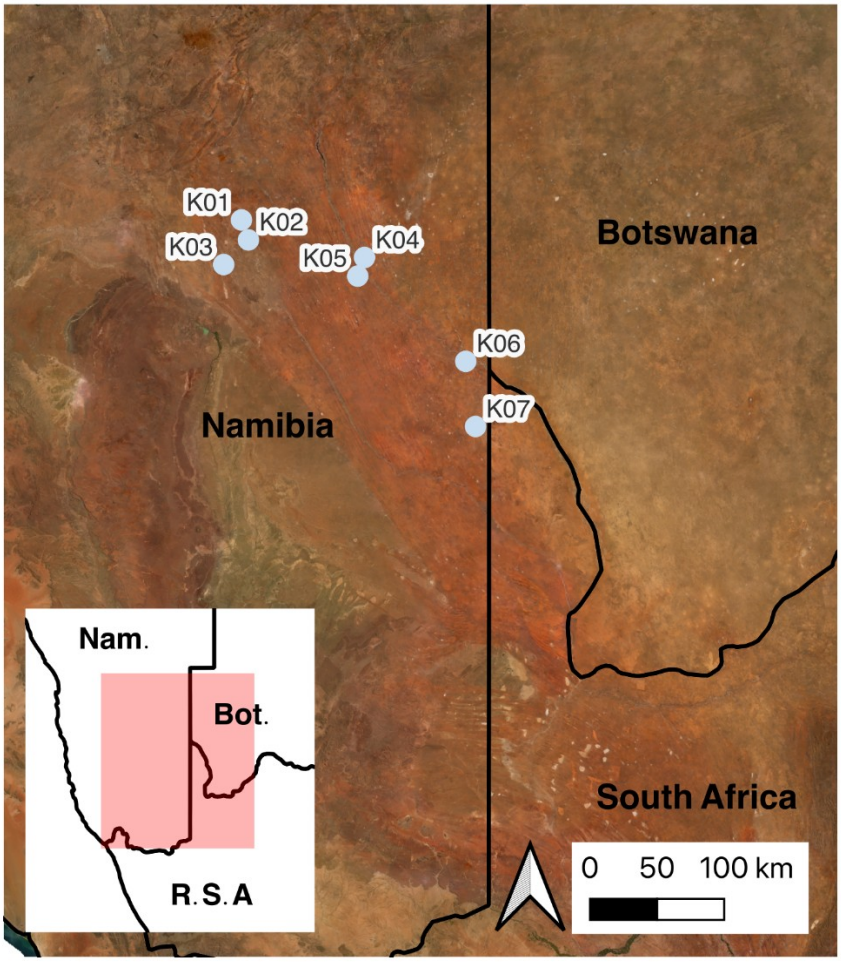

Figure 1. Locations of sites (K01-K07; see Table 1). Background imagery © 2023 Planet Labs PBC (Planet, 2023).

The linear dune system lies within the southern Africa summer rainfall zone and has a mean annual precipitation of 150 – 300 mm but, characteristic of dryland regions, interannual variability is high at 50 % (Thomas and Leason, 2005; Bhattachan et al., 2014). The rain generally falls between November and April; accordingly, September and October represent the end of the dry season. Additionally, the end of the dry season also coincides with the windiest months (Nchaba et al., 2017; Bullard et al., 1996). In the 12 months preceding September 2022 when measurements were made, the sites received an average of 201 mm precipitation.

The fire season peaks in September but can continue into the early wet season. Fires in the region are limited by vegetation, which provides both fuel and affects the connectivity of the burnable surface. Vegetation mass and extent is strongly linked to precipitation and to land use (Andela et al., 2019). Consequently, like precipitation, fires have a high interannual variability, and occur regularly after wetter La Niña periods which provides the moisture for biomass build up (Chen et al., 2017).

The typical vegetation in the study area is Kalahari Xeric Savanna (van Rooyen and van Rooyen, 1998), with varying surface coverage depending on land use history. The vegetation composition on the dunes is a mix of annual grasses (mainly *Schmidtia kalahariensis)*, perennial grasses (e.g., *Stipagrotis amabilis*), prostrate creepers (e.g., *Aptosimum elongatum*), patches of shrubs (e.g., *Lycium hirsutum*) and sporadically populated trees (e.g., *Acacia haematoxylon*). All measurements were conducted on farmland which is either sheep, goat, or cattle grazed. Most of the unburned farmland had a high coverage of annual grasses.

Biological soil crusts (biocrusts) were observed at each site and in burned interdune plots. This observation aligns with previous work in the region noting that biocrusts cover between 11 to 95 % of the ground surface, with its high variability being attributed to disturbance history (Thomas and Dougill, 2007). Additional studies have observed that biocrust cover is ubiquitous across Kalahari surfaces (Elliott et al., 2014, 2024; Lan et al., 2021; Thomas and Dougill, 2006; Mager, 2010; Dougill and Thomas, 2004). However, the absence of surface discolouration reduced the field visibility of the biocrust, making it not possible to reliably quantify its presence. This

was due to the lack of surface discolouration in the early stages of biocrust development (Bullard et al., 2022; Dougill and Thomas, 2004). No physical crusts were observed at the experimental sites.

2.2. Experimental set-up

Seven burned sites, with different fire ages (Time Since Fire: TSF), were identified using remote sensing, followed by conversations with local landowners (Table 1 and Figure 1). Each burned site was co-located with a nearby unburned control site. Where possible the site pairs (burned and control) were close to each other on the same dune (typically within 1 km of each other), or on the adjacent interdune. The sites were then further divided into plots to investigate the effect of the dune morphological unit on emission potential with particular focus on the dune crest and interdunes (Figure 2). The different morphological positions of the plots on the dune surfaces are summarised in Table 1. The accessibility of the area burned limited the ability to record at all the dune topographies. From herein, 'site' refers to the broader burned area and the co-located control area and 'plot' refers to the experimental area within a site in a distinct dune morphological unit.

All the measurements took place on grazed-disturbed land. Trampling by the grazing animals is known to break-up the surface and disrupt biocrusts (Thomas and Dougill, 2007). To evaluate the significance of the biocrust on erodibility, surfaces at each plot were disturbed by removing the top two centimetres using a spade, removing the biocrust. Herein, the plots where the surface was removed are termed 'scraped plots'. Once the surface sediments , including any biocrust, were removed, additional PI-SWERL measurements were made (Figure 2). The surface

scraping was not intended to replicate any particular real-world disturbance but instead was aimed at identifying whether biocrust presence impacted on sediment availability. Subsequently, the maximum number of experimental plots at each site was nine - the burned crest, flank, and interdune, with co-located control plots and additional scraped interdune, flank, and crest plots.

Table 1. Location, date of fire, and plot position for each burned site

Site	Latitude	Longitude	Date of fire	TSF (months)	Dune morphology measured
K01	-23.722675	18.109997	01/09/2022	0 and 1	C*, F, ID
K02	-23.8606	18.1507	26/07/2022	1	C, ID
K03	-24.04225	17.98124	18/06/2022	4	C, ID
K04	-23.98248	19.01717	29/11/2021	10	C, F, ID
K05	-24.1159	18.99656	16/11/2021	10	ID
K06	-24.68887	19.82227	27/10/2020	25	C, ID
K07	-25.185	19.8947	28/02/2012	127	ID

C – Crest, F – Flank, ID – Interdune
**Control only*

	Burned	Control
Crest		
Flank		

Figure 2. Examples of PI-SWERL measurement locations on different topographies.

2.3. Grain size distribution

One surface sediment sample was taken per measurement plot (Table 1) for laboratory analysis. Grain size distribution measurements for samples were conducted using the wet (no pre-treatment) dispersal method with a Malvern Mastersizer Hydro 2000MU laser diffraction particle size analyser. Before analysis, samples were oven dried overnight and sieved to less than 2 mm and exposed to 10 s of ultrasonic dissolution, with the ultrasound setting at 10 µm. Samples were then classified by type where clay is <2 µm, silt is 2 µm to 50 µm, and sand is 50 µm to 2000 µm. In addition, to classify grains that have the sedimentary potential to be emitted as dust at the surface, sediment was further classed into particles which are inhalable under 10 µm and super-coarse dust particles under 62.5 µm. These sizes were chosen as < 10 µm aligns with the measurements made with the PI-SWERL and < 62.5 µm is the size bracket identified by Adebiyi et al. (2023) as currently underestimated in the atmosphere. Kruskal-Wallis chi-squared tests were used to

assess any statistical differences between the different morphological units where measurements were taken on the dune (i.e., crest, flank, and interdune) and grain size distribution.

2.4. PI-SWERL measurements

Emission flux was measured using the Portable In-Situ Wind Erosion Laboratory (PI-SWERL ®; DustQuant LLC, Las Vegas, NV, USA), now a widely used technique (Bacon et al., 2011; Sweeney and Mason, 2013; Vos et al., 2021; King et al., 2011; Walker et al., 2023; Kolesar et al., 2022; von Holdt et al., 2019; Wang et al., 2025). The instrument (as seen in Figure 2) consists of a flat, annular ring inside a closed chamber rotating about 6.5 cm above the ground which exerts shear stress on the surface and entrains particles. The emitted particles are measured by a DustTrak ® II model 8530 nephelometer to measure the PM_{10} concentration of dust in the chamber per second in mg m^{-3}. Fresh air is pumped into the chamber at a rate of approximately 0.1 m^{-3} s^{-1}. The PI-SWERL was preprogramed to run at a variety of revolutions per minute (RPM) which translate into specific friction velocities (u_* m s^{-1}). The relationship between RPM and u_* is determined by surface roughness and defined as:

$$u_{i\,eff}(RPM) = C_1 \cdot \alpha^4 \cdot RPM^{C_2/\alpha}$$

Equation 1

where, C_1 and C_2 are constants 0.000683 and 0.832 respectively (Etyemezian et al., 2014). α is a value calculated based on surface roughness using the look-up table in Hartshorn et al. (2023). It was deemed that all surfaces consisted of loose

unconsolidated sand which was less than 2.5 % gravel cover, therefore, the α value of 0.98 was chosen for all sites, equating to a peak u_* value of 0.64 m s^{-1} at 3500 RPM. This u_* value was chosen to account for high wind velocity events previously identified in the dune field by Wiggs et al. (1994).

The rotation of the flat ring was increased at a constant rate (ramp test). The ramp test was chosen as it enables the determination of (a) if the plot is capable of emitting dust, (b) enables an easy identification of the erosion threshold, and (c) any changes in dust emission flux whilst at a constant rate. At the start of each test, a 60 s clean air run was undertaken to flush out any remaining particles in the chamber (Figure 3). The RPM was then increased from 0 to 3500 RPM over 90 s, held at 3500 RPM for 120 seconds, and then reduced to 0 RPM together with a clean air flush for the final 60 seconds of the test (Figure 3). To reduce contamination between each run, the inside of the chamber was brushed down to remove any remaining visible sediment and after concluding measurements at each plot, the PI-SWERL was run at max RPM for three minutes.

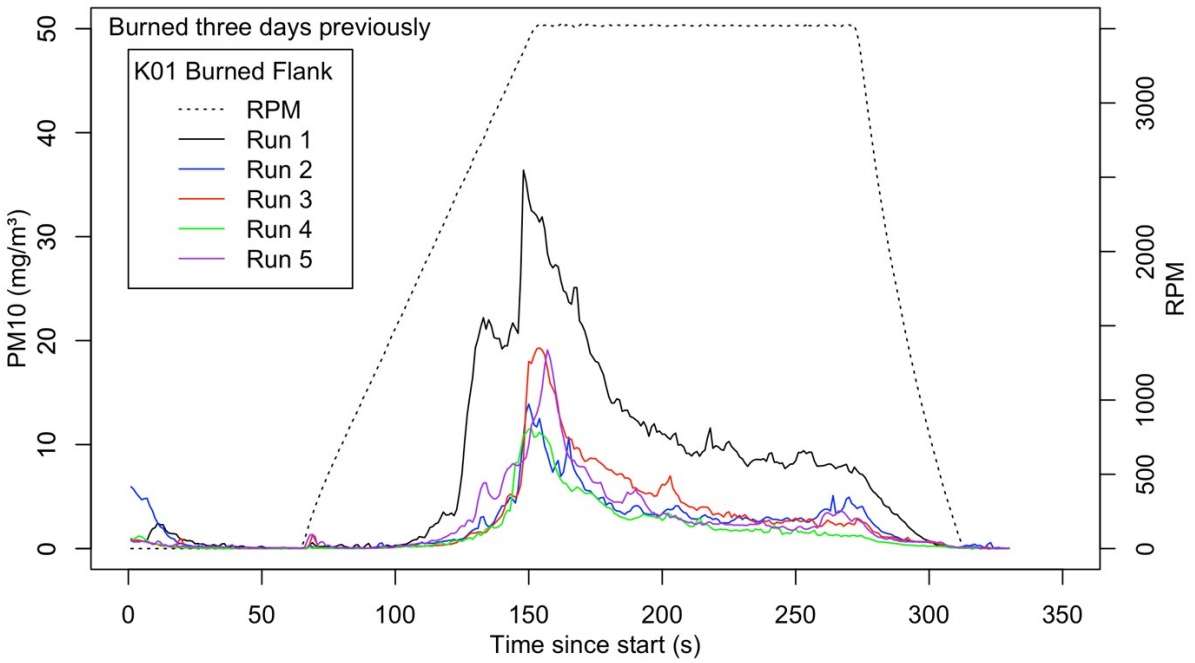

Figure 3. Example runs of a PI-SWERL at each measurement plot, displaying the programming used for each measurement.

Many previous experiments with a PI-SWERL have utilised a 'step' test, where the flux of dust is measured at different u_* to assess differing wind velocities (e.g., Bacon et al., 2011; Cui et al., 2019; Sankey et al., 2012). As the aim of this study is to assess the potential for the surface to be emissive, and if there is any change in thresholds with different disturbances only one maximum velocity is used. This maximum RPM was maintained for 90 s (Figure 3), which allows us to calculate flux and identify controls on emission.

Threshold of emission (u_{*T}) was determined using the same process as Cui et al. (2019) and van Leeuwen et al. (2021) where the first recording when the PM_{10} concentration began to consistently increase for ten or more seconds is determined as the threshold. The threshold RPM was then converted into u_* using the Equation 1. The PM_{10} flux was calculated using the equation:

$$E_i = \frac{\sum_{begin,i}^{end,i} C \cdot F}{\left(t_{end,i} - t_{begin,i}\right) \cdot A_{eff}}$$

Equation 2

where C is the measured PM_{10} concentration (mg m^{-3}), F is the airflow rate (L s^{-1}), t is the duration (s) of step i, and A_{eff} is the effective area (m^2) of the PI-SWERL (0.035 m^2; Sweeney et al., 2011; Etyemezian et al., 2014). The flux was used to compare emission fluxes to other measurements and PI-SWERL results.

Within each plot, a ten metre transect was set out and a PI-SWERL measurement was taken every two metres along the transect. At each plot the biocrust was removed at a plot away from the transect for further PI-SWERL measurements to be conducted. One to six measurements were performed at each plot to get a representative characterisation of the surface (Table 2). A smaller number of measurements were performed at a plot if the peak concentrations of dust flux in the initial measurements were consistent (within a tolerance of 5 mg m^{-3}). If there was grass and creeper coverage, to ensure that the vegetation did not interfere with the rotating blade, vegetation was trimmed using shears to surface level (Figure 2), taking care not to disturb the surface. In total, 180 Pi-SWERL measurements were conducted at seven sites during September and October 2022 (Table 2).

Table 2. Measurements made at each plot. C denotes a control plot and B denotes a plot which has burned. Scraped surfaces are where the top 2 cm of the surface was removed. K01 was visited twice, three days after burning and then 1 month after burning.

	K01 (3 Days)	K01 (1 month)	K02	K03	K04	K05	K06	K07
Interdune (C)	5		5	5	5	5	5	4
Interdune (B)	5	5	5	5	5	3	5	5
Flank (C)	5				5			
Flank (B)	5	5			5			
Crest (C)	3		5	5	5		6	
Crest (B)			5	5	5		4	
Scrape -Interdune	3	2	3	4	6		6	1
Scrape -Flank	6							
Scrape -Crest							3	

The PM_{10} threshold and flux data were analysed to determine statistical differences based on dune morphological unit (dune morphological unit, i.e., crest, flank, and interdune) and status (burned or control). The choice of statistical test depended on the data distribution and number of groups compared. Kruskal-Wallis chi-squared tests were used to assess differences in emission flux across dune morphological units and status (i.e., control, burned, or scraped), while Welch Two Sample t-tests were applied to threshold data for the same factors. Additionally, for variations in measurements taken at different dune morphological units, Kruskal-Wallis chi-squared tests were used for emission flux, and Analysis of Variance (ANOVA) was applied to threshold data.

3. Results

3.1. Sediment Size distribution

88.4 % of the samples have a soil texture of sand, the remaining 11.6 % is classified as sandy loam. Only 5.8 % contained any clay sized (< 2 µm) material and 92.8 %

containing silt sized (2 - 50 µm) material. Differences can be observed when assessing the topographical location of the sediments. 30 % of crest plots contained sediment smaller than 10 µm, whilst all the interdune plots have a higher percentage of sediment under 10 µm (with a maximum content of 8.9 % at K01 burned interdune plot).

Sediment finer than 62.5 µm is typically considered to be able to be suspended in the atmosphere (Adebiyi et al., 2023). The proportion of sediment under 62.5 µm differed significantly with the different dune morphological unit (Kruskal-Wallis $p < 0.0001$). Interdunes had the largest mean proportion of sediment < 62.5 µm at 9.8 %, whilst the flanks had 4.3 % and the crests had 1.7 % on average (Table 3).

348

349 **Table 3.** Grain size data for samples from the study plots.

		% of sample																		
		Clay				Silt				Sand				< 10 µm				< 62.5 µm			
		$\overline{x}$	Max.	Min	SD	$\overline{x}$	Max.	Min.	SD	$\overline{x}$	Max.	Min.	SD	$\overline{x}$	Max.	Min.	SD	$\overline{x}$	Max.	Min.	SD
	C	0.0	0.0	0.0	0.0	2.6	7.3	1.3	1.9	97.4	98.7	92.7	1.9	0.6	2.0	0.0	0.6	3.2	9.5	1.3	2.6
	F	0.0	0.0	0.0	0.0	2.6	3.2	1.4	1.5	97.4	96.8	95.2	1.5	1.4	1.7	0.3	0.6	4.2	6.9	2.0	2.0
Burned	ID	0.0	0.1	0.0	0.0	9.2	25.3	1.6	6.9	90.7	98.4	74.7	6.9	2.9	8.9	0.2	2.3	11.4	30.0	2.1	8.2
	C	0.0	0.0	0.0	0.0	0.4	0.8	0.0	0.3	99.7	100.0	99.2	0.3	0.0	0.0	0.0	0.0	0.6	1.4	0.0	0.4
	F	0.0	0.0	0.0	0.0	3.6	7.0	0.0	2.8	96.5	100.0	93.0	2.8	1.2	2.8	0.0	1.1	4.4	8.2	0.0	3.4
Control	ID	0.0	0.0	0.0	0.0	6.0	11.9	1.0	3.0	94.0	99.0	88.1	3.0	1.8	3.4	0.1	1.0	7.6	14.7	1.4	3.7

C- Crest, F- Flank, and ID - Interdune

350

3.2. The impact of dune topography on emission threshold and flux

There was great variance in both u_{*T} and emission flux with the location of the plots on the dune (Table 4). The dune morphological unit is highly significant for both the u_{*T} (ANOVA, $p < 0.01$) and the flux of dust (Kruskal-Wallis test, $p < 0.01$). Of the undisturbed surfaces, interdunes had the largest peaks in emission, with the unburned interdune at K07 recording a PM_{10} peak concentration of 65.5 mg m^{-3} (with a flux of 1.892 mg m^{-2} s^{-1}). Yet, on average the flanks of the dunes have the largest flux of dust (Figure 4b). However, scraped surfaces consistently saw the highest fluxes of dust (Figure 4), recording a peak concentration of 173 mg m^{-3} (with a flux of 6.305 mg m^{-2} s^{-1}) observed at K02 scraped interdune.

Table 4. Descriptive statistics of measured threshold velocities (m s^{-1}) and emission flux (mg m^{-2} s^{-1}) for each dune morphological unit and disturbance type.

Dune morph. unit	Disturbance	n	Threshold (m s^{-1})				Flux at 0.64 m s^{-1} (mg m^{-2} s^{-1})			
			$\overline{x}$*	SD*	Min	Max	$\overline{x}$*	SD*	Min	Max
ID	B	38	0.308	1.305	0.187	0.551	0.190	3.363	0.005	1.892
	C	34	0.221	1.610	0.038	0.462	0.281	3.061	0.005	1.587
	S	25	0.167	2.670	0.187	0.409	1.105	2.033	0.862	6.305
Flank	B	15	0.264	1.228	0.202	0.417	0.403	1.942	0.129	1.251
	C	10	0.175	2.525	0.013	0.391	0.447	2.397	0.069	0.999
	S	6	0.266	1.218	0.202	0.310	1.949	1.815	0.500	2.538
Crest	B	19	0.303	1.298	0.179	0.489	0.467	1.430	0.029	0.723
	C	24	0.282	1.414	0.178	0.424	0.253	2.428	0.238	0.960
	S	3	0.288	1.601	0.210	0.495	0.942	1.026	0.923	0.970

**Geometric Mean and Standard Deviation*
B = Burned, C = Control, and S = Scraped (biocrust removed)

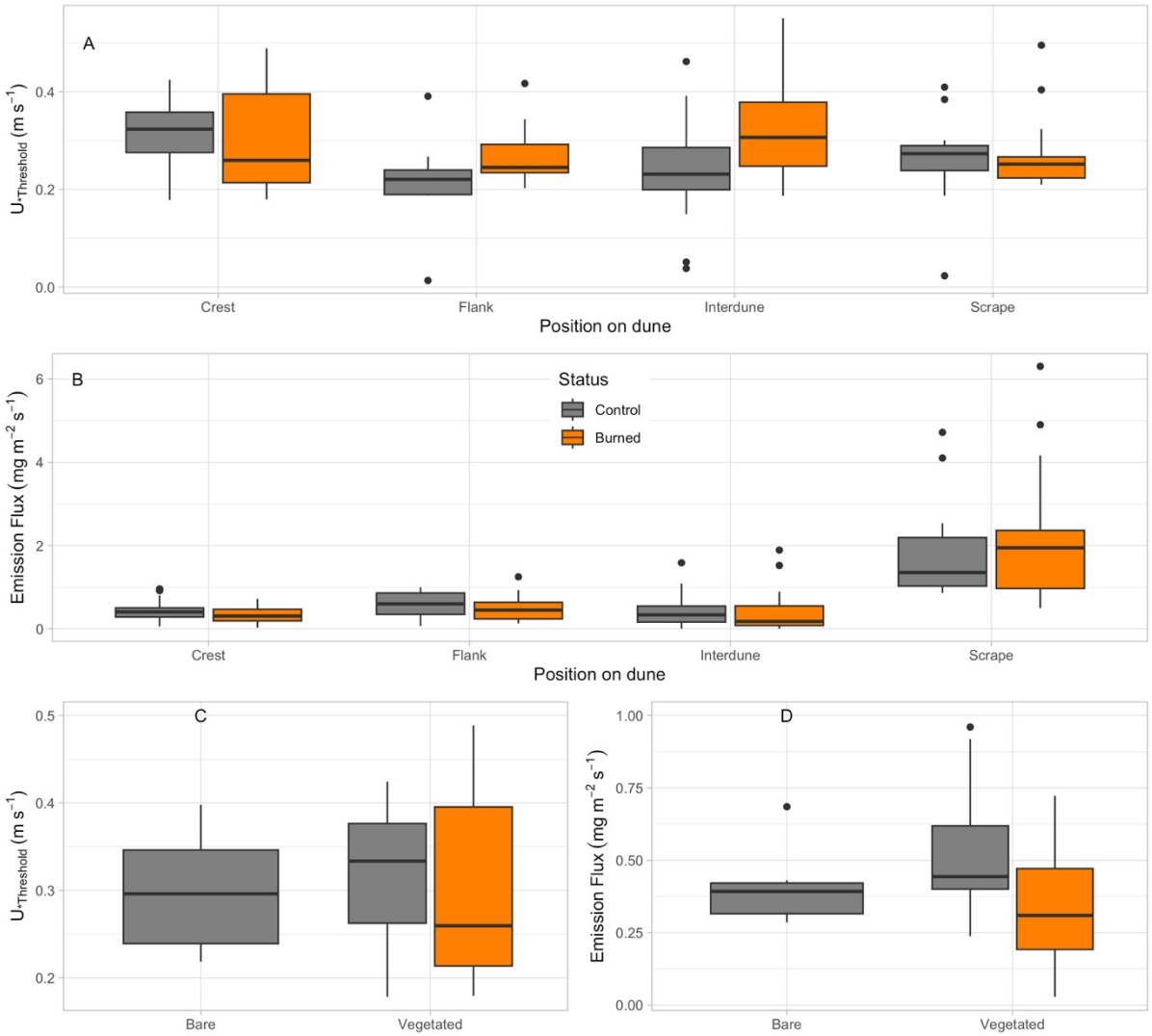

Figure 4. Panels A and B: u_{*T} and emission flux for the crests, flanks, interdunes, and scraped (biocrust removed) surfaces across all the measurement plots. Panels C and D: u_{*T} and emission flux for the crest plots only subdivided into bare and vegetated crest plots. Burned plots are in orange and control plots are displayed in grey.

3.3. Inter-plot comparisons

Each plot investigated has different surface properties that impact the ability to emit dust, and there is a significant difference in the emission flux between each control interdune plot (Kruskal-Wallis test, $p < 0.01$). Emission fluxes from each experimental plot are reported in Table 5. There was no significant difference in the flux between the control crests and flanks between the sites. All control plots showed

379 similar u_{*T} values (Figure 5), which are not significantly different from one another
380 (ANOVA, $p > 0.05$) in contrast to the emission flux.

381

382 The significant difference between each control plot made isolating the evolution of
383 dust emission with time since fire difficult. Further, there is no distinct pattern in
384 whether the burned or control plots had high emission fluxes or emission thresholds
385 with time since fire (Figure 5). Subsequently, there are no further investigations into
386 dust emission potential over time as burned areas heal.

387

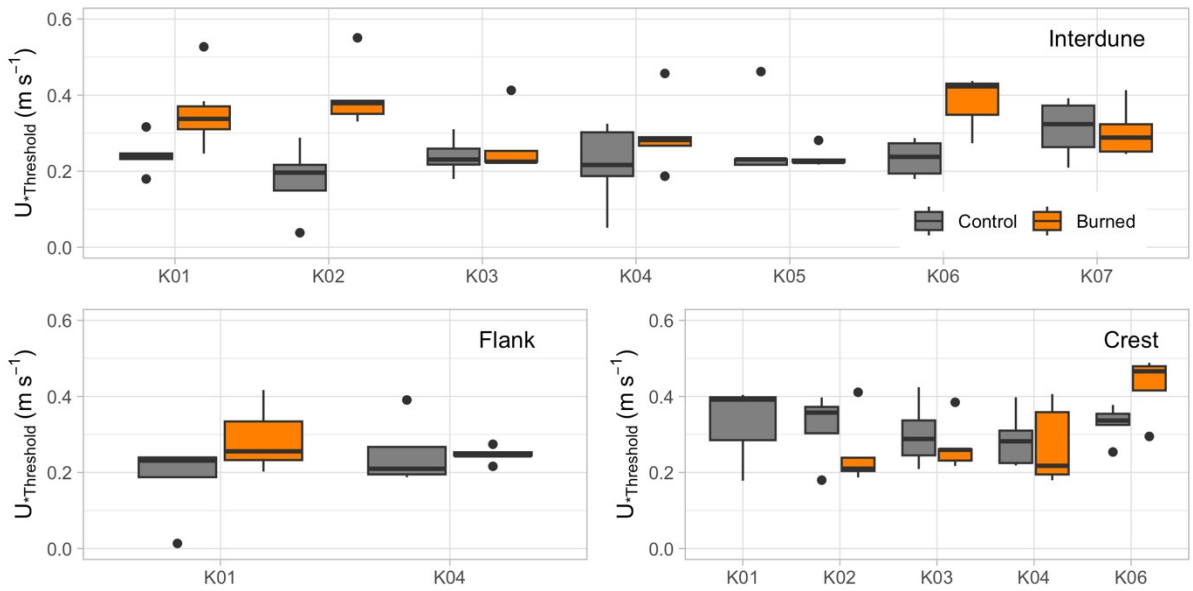

388

389 **Figure 5.** u_{*T} at each site on the interdune, flank, and crest plots.

390
391 **Table 5.** Emission flux for each experimental plot measured.

	Emission flux (mg m^{-2} s^{-1}) (geometric mean ± geometric standard deviation)							
	K01 (3 days)	**K01 (1 month)**	**K02**	**K03**	**K04**	**K05**	**K06**	**K07**
Interdune (C)	0.936 ± 1.442		0.065 ± 6.192	0.406 ± 1.659	0.237 ± 1.789	0.176 ± 2.324	0.303 ± 1.529	0.487 ± 1.514

Interdune (B)	0.108 ± 1.570	0.035 ± 3.249	0.221 ± 3.108	0.653 ± 1.235	0.197 ± 1.711	0.273 ± 1.897	0.065 ± 1.509	0.575 ± 3.336
Flank (C)	0.713 ± 1.340				0.280 ± 2.840			
Flank (B)	0.268 ± 1.691	0.322 ± 1.792			0.756 ± 1.489			
Crest (C)	0.893 ± 1.095		0.454 ± 1.318	0.449 ± 1.085	0.353 ± 1.210		0.451 ± 1.486	
Crest (B)			0.367 ± 2.290	0.384 ± 1.246	0.297 ± 1.495		0.078 ± 2.862	
Scrape - Interdune	2.245 ± 1.167	4.400 ± 1.104	5.007 ± 1.247	1.747 ± 2.021	1.732 ± 1.306		1.052 ± 1.119	1.872
Scrape - Flank	1.105 ± 2.033							
Scrape - Crest							0.942 ± 1.026	

3.4. The effect of burning on emission threshold and flux

The magnitude of difference in dust flux between the burned and control plot varies with site (Figure 5). In the interdunes, four plots had higher concentrations of dust in the control plot and four had higher concentrations in the burned area (Figure 6). The difference between the burned and control plots are minimal as four plots have overlapping standard deviations (Figure 6 – panel C, D, E, H).

The burned and control surfaces had significantly different u_{*T} (T-test, $p < 0.01$) on all topographies, with burned sites having a higher threshold for erosion. In contrast, burning does not have a significant impact on the emission flux on all topographies (Kruskal-Wallis test, $p > 0.05$). The largest average difference in the flux between the burned and control plots at the same site was found at the interdune K01 where the

difference between the geometric means was 0.901 mg m^{-2} s^{-1} with the control plot having a larger dust flux.

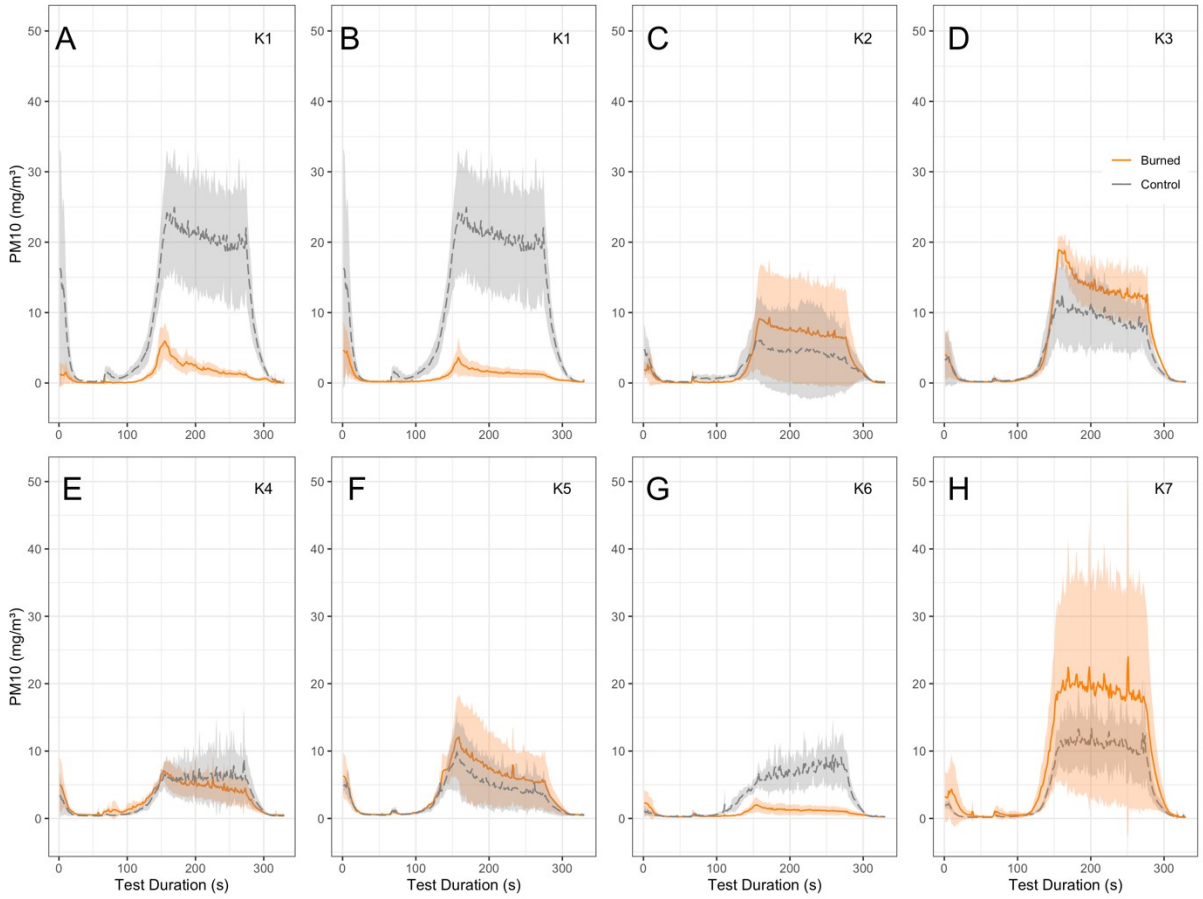

Figure 6. PM_{10} emissions for the burned and control plots at each interdune plot. Mean PM_{10} (mg m^{-3}) concentration is the solid line with one standard deviation shaded. The burned plots are in orange and the control plots are in grey. In A the area was burned three days before measurement and in panel B the plot was remeasured one month after burning, the same control plot data was used for both measurements.

3.5. The effect of biocrust removal on emission threshold and flux

Scraped surfaces where the biocrust was removed constantly reported the highest fluxes of dust (Table 5 and Figure 4b) but similar threshold for emissions (Table 4 and Figure 4a). The ratio of geometric means for burned and scraped interdune plots was 0.08 ± 3.70 and for the unburned and scraped interdune plots was 0.13 ± 1.74 (Table S1). These results indicate that the scraped (biocrust-removed) surfaces produced approximately 8 – 13 times higher dust fluxes than the burned and control surfaces. The largest difference between the control and scraped plots measured was at site K02 where the geometric mean of flux from the control plot was 0.065 mg m^{-2} s^{-1} whereas the biocrust-removed plot had a geometric mean flux of 5.007 mg m^{-2} s^{-1}, 77 times greater than the control plot. The largest flux of dust from any one measurement was recorded on a biocrust-removed surface with a peak flux of 6.305 mg m^{-2} s^{-1} at the burned interdune plot at site K02.

3.6. Summary of results

The Kalahari sediment has up to 9 % of grains by volume with a grainsize of < 10 µm. This is particularly the case in the interdune areas. When tested using the PI-SWERL, all sites displayed some PM_{10} emission, but the threshold for erosion and emission flux varied with the surface status (control/burned/scraped), site, and the morphological unit of the dune. The dune crests had the lowest dust flux with an average emission of 0.253 mg m^{-2} s^{-1} whereas the flanks showed the largest dust flux with an average emission of 0.447 mg m^{-2} s^{-1}. The results of this study show that fine sediment is found in most of the experimental plots. Burning increases the erosion threshold of dune surfaces although this does not significantly impact the flux of

emitted dust (Table 4). Once the biocrust has been removed, dust flux can increase by up to 77 times compared to control and burned surfaces.

4. Discussion

In this study, a wide range of variables (dune morphological unit, burning, and biocrust removal) were tested to assess their impact on dust emission from the southwest Kalahari dune system. Characterisation of emission potential of vegetated dune fields and factors that modulate the baseline emissivity are important to quantify for global emissivity/erodibility maps and models of dust flux, both now and into the future (Kok et al., 2021a). This study presents a broad dataset of potential PM_{10} emissions and estimated threshold velocities from vegetated linear sand dunes and further explores within-dune landscape variations and different disturbance pressures. Overall, results indicate that potential emission of mineral dust is low across all sites in the southwest Kalahari linear dune system regardless of whether the dunes have burned or not. But disturbing the surface through the removal of biocrust results in higher emission fluxes (up to 77 times greater) of dust.

4.1. Fine sediments within dune compositions

Grain size analysis shows that there is fine material (< 62.5 µm) within the sediment composition (ranging from 0 % to 30 %) at most plots measured. Fine grain (< 62.5 µm) presence indicates that if the dunes become de-vegetated the fine grains should be available to be eroded by the wind. This substantiates the observation by

463 Bhattachan et al. (2012) that the Kalahari has the potential to emit dust once de-
464 vegetated.

465

466 4.2. Emission from the southwest Kalahari linear dunes
467 compared to other PI-SWERL tests

468

469 **Table 6.** Measurements of dust flux from sand dunes in previous PI-SWERL studies. If the
470 study reports where on the dune measurements are made the topography is reported,
471 otherwise the terminology used in the study is used. Many studies did not report the α
472 value, if the value is not mentioned a hyphen is used in place. Where studies have multiple
473 measurements of the same surface at different u_* then the closest two u_* values to the current
474 study (0.64 m s^{-1}) are used.

Study	Topography	u_* (m s^{-1})	α value	Emission flux (mg m^{-2} s^{-1})	Metric
Bacon et al., 2011	Crest	0.69	-	4.21 ± 4.72	Geometric mean ± Standard Deviation
Cui et al., 2019	Interdune	0.55	0.96-0.90	~1	Geometric mean
Dickey et al., 2023	Interdune	0.73	0.9	2.30 ± 0.81	Geometric mean ± Standard Deviation
King et al., 2011	Interdune	0.56	-	0.269 ± 1.252	Geometric mean ± Standard Deviation
King et al., 2011	Interdune	0.56	-	0.2 79 ± 1.511	Geometric mean ± Standard Deviation
Kolesar et al., 2022	Active dune	-	-	0.20 ± 0.11	Mean ± Standard Deviation
Sweeney et al., 2018	Coppice	0.7	0.98 - 0.92	~2	Median
Sweeney et al., 2016	Stabilised	0.7	0.98 - 0.92	<0.5	Median
Sweeney et al., 2011	Dune	0.56	-	0.1443	Geometric mean
Sweeney et al., 2022	Vegetated	0.6	0.96	0.356 ± 0.241	Geometric mean ± Standard Deviation
Sweeney et al., 2022	Interdune	0.6	0.88-0.96	0.033 ± 0.063	Geometric mean ± Standard Deviation
Sweeney et al., 2022	Interdune	0.7	0.88-0.96	0.07 0 ± 0.193	Geometric mean ± Standard Deviation
Sweeney et al., 2022	Active	0.6	0.96-0.98	0.048 ± 0.059	Geometric mean ± Standard Deviation
von Holdt et al., 2019	Dune	-	-	0.0640 ± 1.199	Geometric mean ± Standard Deviation
Wang et al., 2025	Active	0 – 0.69	-	0.25	Average
This study	**Interdune (undisturbed)**	**0.64**	**0.98**	**0.28 1 ± 3.061**	**Geometric mean ± Standard Deviation**
This study	**Crest**	**0.64**	**0.98**	**0.253 ± 0.238**	**Geometric mean ±**

	(undisturbed)	Standard Deviation

Comparison of the PI-SWERL data between studies must take account of the respective u* values used. Only one study used the same u* (0.64 m s^{-1}) as this study and used emission fluxes on a variety of different landscapes in the Salton Sea, USA (Dickey et al., 2023). However, all dune measurements by Dickey et al. (2023) reported higher emission flux measurements than both the burned and control plots in the current study. These higher fluxes included surfaces which typically would be expected to have lower flux such as sand with gravel lag (Dickey et al., 2023).

Previous PI-SWERL experiments have found that undisturbed bare sand dunes have a low emission potential when compared to landforms such as dry washes or playas (King et al., 2011; Sweeney et al., 2016) but higher emissions than many other surfaces such as desert pavements and alluvial fans (Dickey et al., 2023). The dust flux measured from the partially vegetated linear dunes in this study is frequently lower than those from dunes in other geographic locations. For example, Sweeney et al. (2023) found a PM_{10} max of 18.99 mg m^{-2} s^{-1} from sand from a stabilised dune in Arizona. This is an order of magnitude higher than the maximum undisturbed flux of 1.89 mg m^{-2} s^{-1} which was recorded at K07 burned interdune plot, however Sweeney et al. (2023) exerted a much higher shear velocity of 0.82 m s^{-1} on the surface compared to this study's 0.64 m s^{-1}. Higher emission fluxes were also observed from dunes in the Salton Sea, USA where an average flux of 2.30 mg m^{-2} s^{-1} was measured at a u_* of 0.73 m s^{-1} (Table 6; Dickey et al., 2023). Other studies have measured similar levels of emission flux to this study, for example in northern China Cui et al. (2019) at a slightly higher u_* of 0.69 m s^{-1} and in the southwest USA by King

et al. (2011) at a lower u_* of 0.56 m s^{-1} (Table 6). The fluxes of dust from the scraped surfaces were of similar magnitude to highly emissive surfaces such as dry washes (King et al., 2011), smooth playas (Dickey et al., 2023) and Wadis (Cui et al., 2019) although the u* values used in these studies ranged from 0.55 to 0.73 m s^{-1}. The similar fluxes indicates that if the biocrust is removed, emission fluxes can be similar to those reported from frequently dust producing topographies.

Notably, there is a wide range of α values used to account for different surface roughness and to calculate u_* used in all PI-SWERL studies. Of the above-mentioned studies, α values range from 0.9 – 0.96 on sand dune surfaces, which affect the u_* value and cross-study comparison. These values were chosen based on a table in Etyemezian et al. (2014). The u_* value is sensitive to the choice in α value. For example, the peak RPM of 3500 was used in this study with a resulting u_* value of 0.64 m s^{-1} at an α value of 0.98, if the α value is changed to 0.9 the u_* value becomes 0.85 m s^{-1}. Recently a visual look up table was created by Hartshorn et al. (2023) and this table was used in the selection of 0.98 as the α value for this study. The new look-up table should reduce the discrepancy in assigning α values and thus u_* estimates into the future.

4.3. Disturbance effects

Factors that are frequently cited as disturbance agents in the arid zone context include drought, fire, and grazing (e.g., Hesse and Simpson, 2006; Mayaud et al., 2016; Nield and Baas, 2008; Wasson and Nanninga, 1986). Drought and fire do not produce any mechanistic changes in sediment distribution at the surface, only

grazing reorganises the sediments through hoof action. In this study, we investigate two types of disturbance, biocrust-removal (scraped surfaces) and environmental (burned surfaces). In previous studies, disturbance has been an umbrella term to show that disturbed surfaces produce a higher flux of dust (Bacon et al., 2011; Cui et al., 2019).

To simulate disturbed biocrust surfaces in the Kalahari largely caused by ungulate hoof action (Thomas and Dougill, 2007) biocrusts were removed by scraping. In these modified plots fluxes were larger (geomean 1.654 mg m^{-2} s^{-1}) than undisturbed (geomean 0.314 mg m^{-2} s^{-1}) and fire disturbed (geomean 0.240 mg m^{-2} s^{-1}) plots. The scraped plots had dust fluxes similar to those of dust emission hotspots such as dry washes and playas (King et al., 2011) and other generalised disturbed surfaces (Cui et al., 2019). The difference between the biocrust-removed and fire or control measurements reveals the stabilising role of biocrusts on dune surfaces.

The survival of biocrusts post-fire is an explanation as to why there is no statistical difference in the potential emission flux between the burned and control plots. The results show that the protective effect of biocrust remains after burning. Biocrust toleration to fire has been found in the USA and Australia (Palmer et al., 2020), but at present there are no studies in southern Africa. Biocrusts in the dune field likely survive burning as the highly combustible vegetation in the Kalahari burns fast (Andela et al., 2019). The rapid combustion of vegetation reduces the amount of heat transferred to the surface sediment, allowing some biocrust to withstand fire (Palmer et al., 2020; Lentile et al., 2006). Even if the heat transfer is fatal to the biocrusts the

results from this study show biocrust do not lose their protective effects. In addition, the presence of biocrusts has previously been shown to limit PI-SWERL-generated dust flux (Vos et al., 2020; Fick et al., 2020) and globally biocrusts are thought to reduce dust emissions by around 60 % (Rodríguez-Caballero et al., 2022).

As noted in figure 4 and section 3.4 the threshold shear velocity (u_{*T}) increases after burning. There is some uncertainty in why this can happen. Given biocrusts were noted at each site, including after burning, and the widespread nature of biocrusts in the southwest Kalahari it can be inferred that the biocrusts play a stabilising role in maintaining the u_{*T}. In addition, the higher u_{*T} in burned plots can result from several other factors, including the 'baking' of the ground surface during burning and infiltration induced sediment sorting.

Several studies have indicated that surface sediments may undergo thermal alteration or 'baking' following fire (Stavi et al., 2017; Agbeshie et al., 2022). This response is attributed to the presence of finer grain fractions in surface sediments, which are more susceptible to structural disruption and cementation at lower combustion temperatures (Agbeshie et al., 2022). However, this phenomenon remains insufficiently investigated in sandy soil systems. The possible 'baking' of the surface also explains the burned plot higher threshold friction velocity.

Similarly, infiltration-driven vertical grain-size sorting occurs in sandy soils, where finer grains accumulate deeper in the sediment profile and could account for the higher dust fluxes with mechanistic disturbance (Lei et al., 2017b, a). Again, these

processes are insufficiently investigated in sandy soil systems. The alteration of the surface through scraping removed any sorted, baked sediments, and biocrusts, leaving the finer sediment exposed. The removal of these factors together or in isolation may have driven the higher dust fluxes (Figure 4b), indicating that there is the potential for the southwest Kalahari to emit dust.

The higher u_{*T} post-burn is in contrast to previous findings where PI-SWERL measurements in semi-arid shrubland has shown that desert surfaces have higher emissivity after fire (Sankey et al., 2011, 2012). The emissions recorded in Sankey et al., (2012) were concentrated in hotspots under shrubs and were likely due to burn-induced soil hydrophobicity under the shrub canopies (Ravi et al., 2007, 2006). The experimental design for the current study intentionally did not conduct wind tunnel tests under shrubs due to woody vegetation burning incompletely, increasing the surface roughness, and subsequently the shrubby areas would likely not emit dust (see Figure 7).

Figure 7. An example of a burned formerly shrubby area three months after fire at K03. The remaining shrubs increase surface roughness and reduce the likelihood of the location emitting dust.

4.4. The impact of the dune morphological unit on emission flux

The dust flux, erosion threshold, and grain size differ significantly with the dune morphological unit (Figures 4 and 5, Tables 3, 4, and 5), consequently results were divided into the morphological units of crest, flank, and interdune. Overall, the PI-SWERL emission flux results suggest that all morphological units have the potential of emitting low level dust emissions (Table 4). The minimum flux of dust recorded in this study was 0.005 mg m^{-2} s^{-1} at the burned interdune of site K01 one month after burning (Table 4), demonstrating that, even though this is low, the surface can emit some PM_{10}. The interdunes had the largest range of emission flux, and the highest maximum flux of the dune morphological units (1.892 mg m^{-2} s^{-1} at the burned interdune K07 plot), but this was not reflected in the geometric mean where the emissions were mostly lower than the flanks and crests (Table 4). In previous work

in the Kalahari, Bhattachan et al. (2012) discounted the crests of the dunes from being dust-emitting surfaces. Instead, the results from this study suggests that both the flanks and crests have some capacity to emit dust and should be included in dune-field scale estimates of dust emission flux.

On the crests, there was a 1.8 times greater emission flux from the average burned (0.467 m s^{-1}) than the control (0.253 m s^{-1}) plots. The higher flux for emission on burned dune crests is likely an indicator of sediment size distribution rather than the effect of fire. In the Kalahari, many dune crests are not vegetated, if a crest burned it must have had vegetation cover sufficient to allow the spread of fire. Therefore, as vegetation traps allochthonous dust and allows some pedogenesis (Garcia-Pichel et al., 2016; Weber et al., 2022; Garzanti et al., 2022; Gonzales et al., 2018), the burned crest have some finer sediment fraction available to be eroded by the wind. Finer material in burned crests was reflected in our sediment size distributions as the burned crest plots had an average of 2.6 % silt content whereas the control crest plots had an average of 0.3 %. This finding substantiates previous work which has highlighted that vegetated dune fields have a higher potential to emit dust, if denuded of vegetation, than active dune fields (Bullard et al, 2011; Sweeney et al., 2023).

5. Conclusions

The aims of this study were to (1) establish whether the southwest Kalahari dunes have a sedimentary potential to emit dust, and (2) quantify whether the burning of dune vegetation has a significant effect on dust emission. Through utilising surface

sediment sampling and portable wind-tunnel experiments on co-located burned and unburned control plots, we present the first quantification of the impact of fire on the dust emission potential of partially vegetated dune systems. The principal findings from this study are:

1. Up to 9 % of grains by volume in Kalahari dune field surface sediments are smaller than 10 µm, particularly in the interdune areas. This indicates the potential for dust emission from the southwest Kalahari dune field.
2. Burning increases the erosion threshold of dune surfaces although burning does not significantly impact the measured flux of emitted dust.
3. The stabilising role biological soil crusts is indicated by an average 8-13 times higher dust emission potential from scraped surfaces.

The findings from this study highlight the complex biogeomorphic interactions that govern arid desert dune systems. In the southwest Kalahari, vegetation is not the sole stabilising factor that prevents dust from being emitted from the dunes. Instead, biological soil crusts provide surface stabilisation in de-vegetated landscapes. This finding is critical to dune evolution and dust emission models. The role of biocrusts in suppressing desert dust emission worldwide is poorly quantified and future work should aim to enhance our understanding on dust-biocrust interactions. Further, other factors may govern post-fire dust emissions, such as infiltration sediment sorting and the 'baking' of sediments. These factors are poorly constrained and need to be investigated to quantify their role in dust emission from partially vegetated dune fields.

Data availability: The raw PI-SWERL experimental data have been placed on an open-access repository and can be found at the following DOI: 10.5281/zenodo.15470969. The grain size distribution data can be accessed upon request.

Acknowledgements: This research was supported by the University of Oxford Clarendon Scholarship, the Postgraduate Research Award from the Royal Geographical Society (with IBG), the International Association of Sedimentologists Postgraduate Research Grant Scheme, the Geological Society of London, and the Gill Harwood Memorial Fund from the British Sedimentological Research Group. The authors would like to thank the owners of the lands upon which this work was conducted. The authors would like to thank the two reviewers for their valuable comments and suggestions in improving this manuscript.

Bibliography

Adebiyi, A. A., Kok, J. F., Murray, B. J., Ryder, C. L., Stuut, J. B. W., Kahn, R. A., Knippertz, P., Formenti, P., Mahowald, N. M., Pérez García-Pando, C., Klose, M., Ansmann, A., Samset, B. H., Ito, A., Balkanski, Y., Di Biagio, C., Romanias, M. N., Huang, Y., and Meng, J.: A review of coarse mineral dust in the Earth system,

https://doi.org/10.1016/j.aeolia.2022.100849, 2023.

Agbeshie, A. A., Abugre, S., Atta-Darkwa, T., and Awuah, R.: A review of the effects of forest fire on soil properties, J. For. Res., 33, 1419–1441, https://doi.org/10.1007/s11676-022-01475-4, 2022.

Andela, N., Morton, D. C., Giglio, L., Paugam, R., Chen, Y., Hantson, S., Van Der Werf, G. R., and Anderson, J. T.: The Global Fire Atlas of individual fire size, duration, speed and direction, Earth Syst. Sci. Data, 11, 529–552, https://doi.org/10.5194/essd-11-529-2019, 2019.

Bacon, S. N., McDonald, E. V., Amit, R., Enzel, Y., and Crouvi, O.: Total suspended particulate matter emissions at high friction velocities from desert landforms, J. Geophys. Res. Earth Surf., 116, 1–17, https://doi.org/10.1029/2011JF001965, 2011.

Baddock, M. C., Boskovic, L., Strong, C. L., McTainsh, G., Bullard, J. E., Agranovski, I., and Cropp, R.: Iron-rich nanoparticles formed by aeolian abrasion of desert dune sand, Geochemistry, Geophys. Geosystems, 14, 3720–3729, https://doi.org/10.1002/ggge.20229, 2013.

Bhattachan, A., D'Odorico, P., Baddock, M. C., Zobeck, T. M., Okin, G. S., and Cassar, N.: The Southern Kalahari: A potential new dust source in the Southern Hemisphere?, Environ. Res. Lett., 7, https://doi.org/10.1088/1748-9326/7/2/024001, 2012.

Bhattachan, A., D'odorico, P., Dintwe, K., Okin, G. S., and Collins, S. L.: Resilience and recovery potential of duneland vegetation in the southern Kalahari, 5, 1–14, https://doi.org/10.1890/ES13-00268.1, 2014.

Bhattachan, A., D'Odorico, P., and Okin, G. S.: Biogeochemistry of dust sources in Southern Africa, J. Arid Environ., 117, 18–27,

https://doi.org/10.1016/j.jaridenv.2015.02.013, 2015.

Bhattachan, A., Tatlhego, M., Dintwe, K., D'Odorico, P., and Okin, G. S.: Evaluation of dust production efficiencies in sandy sediments, Earth Surf. Process. Landforms, 1–9, https://doi.org/10.1002/esp.5312, 2022.

Buckley, R. C.: Parallel dunefield ecosystems: southern Kalahari and central Australia, J. Arid Environ., 4, 287–298, https://doi.org/10.1016/s0140-1963(18)31475-7, 1981.

Bullard, J. E. and White, K.: Dust production and the release of iron oxides resulting from the aeolian abrasion of natural dune sands, Earth Surf. Process. Landforms, 30, 95–106, https://doi.org/10.1002/esp.1148, 2005.

Bullard, J. E., Thomas, D. S. G., Livingstone, I., and Wiggs, G. F. S.: Wind energy variations in the Southwestern Kalahari desert and implications for linear dunefield activity, Earth Surf. Process. Landforms, 21, 263–278, https://doi.org/10.1002/(SICI)1096-9837(199603)21:3<263::AID-ESP627>3.0.CO;2-I, 1996.

Bullard, J. E., McTainsh, G. H., and Pudmenzky, C.: Aeolian abrasion and modes of fine particle production from natural red dune sands: An experimental study, Sedimentology, 51, 1103–1125, https://doi.org/10.1111/j.1365-3091.2004.00662.x, 2004.

Bullard, J. E., Baddock, M. C., McTainsh, G., and Leys, J.: Sub-basin scale dust source geomorphology detected using MODIS, Geophys. Res. Lett., 35, 1–6, https://doi.org/10.1029/2008GL033928, 2008.

Bullard, J. E., Harrison, S. P., Baddock, M. C., Drake, N., Gill, T. E., McTainsh, G., and Sun, Y.: Preferential dust sources: A geomorphological classification designed

for use in global dust-cycle models, J. Geophys. Res. Earth Surf., 116, https://doi.org/10.1029/2011JF002061, 2011.

Bullard, J. E., Strong, C. L., and Aubault, H. A. P.: Cyanobacterial Soil Crust Responses to Rainfall and Effects on Wind Erosion in a Semiarid Environment, Australia: Implications for Landscape Stability, J. Geophys. Res. Biogeosciences, 127, https://doi.org/10.1029/2021JG006652, 2022.

Chappell, A., Webb, N. P., Hennen, M., Schepanski, K., Ciais, P., Balkanski, Y., Zender, C. S., Tegen, I., Zeng, Z., Tong, D., Baker, B., Ekström, M., Baddock, M. C., Eckardt, F. D., Kandakji, T., Lee, J. A., Nobakht, M., von Holdt, J. R. C., and Leys, J. F.: Satellites reveal Earth's seasonally shifting dust emission sources, Sci. Total Environ., 883, https://doi.org/10.1016/j.scitotenv.2023.163452, 2023.

Chen, Y., Morton, D. C., Andela, N., Van Der Werf, G. R., Giglio, L., and Randerson, J. T.: A pan-tropical cascade of fire driven by El Niño/Southern Oscillation, Nat. Clim. Chang., 7, 906–911, https://doi.org/10.1038/s41558-017-0014-8, 2017.

Cui, M., Lu, H., Wiggs, G. F. S., Etyemezian, V., Sweeney, M. R., and Xu, Z.: Quantifying the effect of geomorphology on aeolian dust emission potential in northern China, 2019.

Dansie, A. P., Thomas, D. S. G., Wiggs, G. F. S., Baddock, M. C., and Ashpole, I.: Plumes and blooms – Locally-sourced Fe-rich aeolian mineral dust drives phytoplankton growth off southwest Africa, Sci. Total Environ., 829, 154562, https://doi.org/https://doi.org/10.1016/j.scitotenv.2022.154562, 2022.

Dickey, H., Schreuder, M., Schmid, B., and Yimam, Y. T.: Quantifying dust emission potential of playa and desert surfaces in the Salton Sea Air Basin, California, United States, Aeolian Res., 60, 100850, https://doi.org/10.1016/j.aeolia.2022.100850, 2023.

748 Dougill, A. J. and Thomas, A. D.: Kalahari sand soils: Spatial heterogeneity,
749 biological soil crusts and land degradation, L. Degrad. Dev., 15, 233–242,
750 https://doi.org/10.1002/ldr.611, 2004.
751 Elliott, D. R., Thomas, A. D., Hoon, S. R., and Sen, R.: Niche partitioning of bacterial
752 communities in biological crusts and soils under grasses, shrubs and trees in the
753 Kalahari, Biodivers. Conserv., 23, 1709–1733, https://doi.org/10.1007/s10531-014-
754 0684-8, 2014.
755 Elliott, D. R., Thomas, A. D., Hoon, S. R., and Sen, R.: Spatial organisation of fungi in
756 soil biocrusts of the Kalahari is related to bacterial community structure and may
757 indicate ecological functions of fungi in drylands, Front. Microbiol., 15, 1–11,
758 https://doi.org/10.3389/fmicb.2024.1173637, 2024.
759 Engelstaedter, S., Kohfeld, K. E., Tegen, I., and Harrison, S. P.: Controls of dust
760 emissions by vegetation and topographic depressions: An evaluation using dust
761 storm frequency data, Geophys. Res. Lett., 30, 30–33,
762 https://doi.org/10.1029/2002GL016471, 2003.
763 Etyemezian, V., Gillies, J. A., Shinoda, M., Nikolich, G., King, J., and Bardis, A. R.:
764 Accounting for surface roughness on measurements conducted with PI-SWERL:
765 Evaluation of a subjective visual approach and a photogrammetric technique,
766 Aeolian Res., 13, 35–50, https://doi.org/10.1016/j.aeolia.2014.03.002, 2014.
767 Fick, S. E., Barger, N., Tatarko, J., and Duniway, M. C.: Induced biological soil crust
768 controls on wind erodibility and dust (PM10) emissions, Earth Surf. Process.
769 Landforms, 45, 224–236, https://doi.org/10.1002/esp.4731, 2020.
770 Field, J. P., Belnap, J., Breshears, D. D., Neff, J. C., Okin, G. S., Whicker, J. J., Painter,
771 T. H., Ravi, S., Reheis, M. C., and Reynolds, R. L.: The ecology of dust, Front. Ecol.

772 Environ., 8, 423–430, https://doi.org/10.1890/090050, 2010.
773 Garcia-Pichel, F., Felde, V. J. M. N. L., Drahorad, S. L., and Weber, B.: Microstructure
774 and Weathering Processes Within Biological Soil Crusts, 237–255,
775 https://doi.org/10.1007/978-3-319-30214-0_13, 2016.
776 Garzanti, E., Pastore, G., Stone, A., Vainer, S., Vermeesch, P., and Resentini, A.:
777 Provenance of Kalahari Sand: Paleoweathering and recycling in a linked fluvial-
778 aeolian system, https://doi.org/10.1016/j.earscirev.2021.103867, 2022.
779 Gill, T.: Airborne dust: A primer for clinicians, Southwest Respir. Crit. Care
780 Chronicles, 6, 4–7, https://doi.org/10.12746/swrccc.v6i22.437, 2018.
781 Ginoux, P., Prospero, J. M., Gill, T. E., Hsu, N. C., and Zhao, M.: Global-scale
782 attribution of anthropogenic and natural dust sources and their emission rates based
783 on MODIS Deep Blue aerosol products, https://doi.org/10.1029/2012RG000388,
784 2012.
785 Gonzales, H. B., Ravi, S., Li, J., and Sankey, J. B.: Ecohydrological implications of
786 aeolian sediment trapping by sparse vegetation in drylands, 11, 1–11,
787 https://doi.org/10.1002/eco.1986, 2018.
788 Hartshorn, E., Sion, B., Sweeney, M. R., and McDonald, E.: Visual Surface Roughness
789 Look-up Table for PI-SWERL Measurements, 2023.
790 Haustein, K., Washington, R., King, J., Wiggs, G. F. S., Thomas, D. S. G., Eckardt, F.
791 D., Bryant, R. G., and Menut, L.: Testing the performance of state-of-the-art dust
792 emission schemes using DO4Models field data, Geosci. Model Dev., 8, 341–362,
793 https://doi.org/10.5194/gmd-8-341-2015, 2015.
794 Hesse, P. and Simpson, R. L.: Variable vegetation cover and episodic sand
795 movement on longitudinal desert sand dunes, 81, 276–291, https://doi.org/10.1016/

j.geomorph.2006.04.012, 2006.

von Holdt, J. R. C., Eckardt, F. D., Baddock, M. C., and Wiggs, G. F. S.: Assessing Landscape Dust Emission Potential Using Combined Ground-Based Measurements and Remote Sensing Data, J. Geophys. Res. Earth Surf., 124, 1080–1098, https://doi.org/10.1029/2018JF004713, 2019.

Jickells, T. D., An, Z. S., Andersen, K. K., Baker, A. R., Bergametti, C., Brooks, N., Cao, J. J., Boyd, P. W., Duce, R. A., Hunter, K. A., Kawahata, H., Kubilay, N., LaRoche, J., Liss, P. S., Mahowald, N. M., Prospero, J. M., Ridgwell, A. J., Tegen, I., and Torres, R.: Global iron connections between desert dust, ocean biogeochemistry, and climate, Science (80-.)., 308, 67–71, https://doi.org/10.1126/science.1105959, 2005.

Kim, D., Chin, M., Schuster, G., Yu, H., Takemura, T., Tuccella, P., Ginoux, P., Liu, X., Shi, Y., Matsui, H., Tsigaridis, K., Bauer, S. E., Kok, J. F., and Schulz, M.: Where Dust Comes From: Global Assessment of Dust Source Attributions With AeroCom Models, J. Geophys. Res. Atmos., 129, https://doi.org/10.1029/2024JD041377, 2024.

King, J., Etyemezian, V., Sweeney, M. R., Buck, B. J., and Nikolich, G.: Dust emission variability at the Salton Sea, California, USA, Aeolian Res., 3, 67–79, https://doi.org/10.1016/j.aeolia.2011.03.005, 2011.

Klose, M., Gill, T. E., Etyemezian, V., Nikolich, G., Ghodsi Zadeh, Z., Webb, N. P., and Van Pelt, R. S.: Dust emission from crusted surfaces: Insights from field measurements and modelling, Aeolian Res., 40, 1–14, https://doi.org/10.1016/j.aeolia.2019.05.001, 2019.

Kok, J. F., Parteli, E. J. R., Michaels, T. I., and Karam, D. B.: The physics of wind-blown sand and dust, Reports Prog. Phys., 75, 106901,

https://doi.org/10.1088/0034-4885/75/10/106901, 2012.

Kok, J. F., Adebiyi, A. A., Albani, S., Balkanski, Y., Checa-Garcia, R., Chin, M., Colarco, P. R., Hamilton, D. S., Huang, Y., Ito, A., Klose, M., Li, L., Mahowald, N. M., Miller, R. L., Obiso, V., Pérez García-Pando, C., Rocha-Lima, A., and Wan, J. S.: Contribution of the world's main dust source regions to the global cycle of desert dust, Atmos. Chem. Phys., 21, 8169–8193, https://doi.org/10.5194/acp-21-8169-2021, 2021a.

Kok, J. F., Adebiyi, A. A., Albani, S., Balkanski, Y., Checa-Garcia, R., Chin, M., Colarco, P. R., Hamilton, D. S., Huang, Y., Ito, A., Klose, M., Leung, D. M., Li, L., Mahowald, N. M., Miller, R. L., Obiso, V., Pérez García-Pando, C., Rocha-Lima, A., Wan, J. S., and Whicker, C. A.: Improved representation of the global dust cycle using observational constraints on dust properties and abundance, Atmos. Chem. Phys., 21, 8127–8167, https://doi.org/10.5194/acp-21-8127-2021, 2021b.

Kok, J. F., Storelvmo, T., Karydis, V. A., Adebiyi, A. A., Mahowald, N. M., Evan, A. T., He, C., and Leung, D. M.: Mineral dust aerosol impacts on global climate and climate change, Nat. Rev. Earth Environ., 4, 71–86, https://doi.org/10.1038/s43017-022-00379-5, 2023.

Kolesar, K. R., Schaaf, M. D., Bannister, J. W., Schreuder, M. D., and Heilmann, M. H.: Characterization of potential fugitive dust emissions within the Keeler Dunes, an inland dune field in the Owens Valley, California, United States, Aeolian Res., 54, 100765, https://doi.org/10.1016/j.aeolia.2021.100765, 2022.

Lan, S., Thomas, A. D., Tooth, S., Wu, L., and Elliott, D. R.: Effects of vegetation on bacterial communities, carbon and nitrogen in dryland soil surfaces: implications for shrub encroachment in the southwest Kalahari, Sci. Total Environ., 764,

https://doi.org/10.1016/j.scitotenv.2020.142847, 2021.

Lancaster, N.: Grain-size characteristics of Linear Dunes in the Southwestern Kalahari, J. Sediment. Petrol., 56, 395–400, 1986.

Langston, G. and McKenna Neuman, C.: An experimental study on the susceptibility of crusted surfaces to wind erosion: A comparison of the strength properties of biotic and salt crusts, 72, 40–53, https://doi.org/10.1016/j.geomorph.2005.05.003, 2005.

van Leeuwen, C. C. E., Fister, W., Vos, H. C., Cammeraat, L. H., and Kuhn, N. J.: A cross-comparison of threshold friction velocities for PM10 emissions between a traditional portable straight-line wind tunnel and PI-SWERL, Aeolian Res., 49, 100661, https://doi.org/10.1016/j.aeolia.2020.100661, 2021.

Lei, X., Yang, Z., He, S., Liu, E., Wong, H., and Li, X.: Numerical investigation of rainfall-induced fines migration and its influences on slope stability, Acta Geotech., 12, 1431–1446, https://doi.org/10.1007/s11440-017-0600-y, 2017a.

Lei, X. qin, Yang, Z. ji, He, S. ming, Liu, E. long, Wong, H., and Li, X. po: Hydro-mechanical analysis of rainfall-induced fines migration process within unsaturated soils, J. Mt. Sci., 14, 2603–2619, https://doi.org/10.1007/s11629-017-4359-2, 2017b.

Lentile, L. B., Holden, Z. A., Smith, A. M. S., Falkowski, M. J., Hudak, A. T., Morgan, P., Lewis, S. A., Gessler, P. E., and Benson, N. C.: Remote sensing techniques to assess active fire characteristics and post-fire effects, Int. J. Wildl. Fire, 15, 319–345, https://doi.org/10.1071/WF05097, 2006.

Mager, D. M.: Carbohydrates in cyanobacterial soil crusts as a source of carbon in the southwest Kalahari, Botswana, Soil Biol. Biochem., 42, 313–318, https://doi.org/10.1016/j.soilbio.2009.11.009, 2010.

Mahowald, N. M., Ginoux, P., Okin, G. S., Kok, J. F., Albani, S., Balkanski, Y., Chin,

M., Bergametti, G., Eck, T. F., Pérez García-Pando, C., Gkikas, A., Gonçalves Ageitos, M., Kim, D., Klose, M., LeGrand, S., Li, L., Marticorena, B., Miller, R., Ryder, C., Zender, C., and Yu, Y.: Letter to the Editor regarding Chappell et al., 2023, "Satellites reveal Earth's seasonally shifting dust emission sources," Sci. Total Environ., 949, 174792, https://doi.org/10.1016/j.scitotenv.2024.174792, 2024.

Mayaud, J. R., Wiggs, G. F. S., and Bailey, R. M.: Characterizing turbulent wind flow around dryland vegetation, Earth Surf. Process. Landforms, 41, 1421–1436, https://doi.org/10.1002/esp.3934, 2016.

McGowan, H. A. and Clark, A.: A vertical profile of PM10 dust concentrations measured during a regional dust event identified by MODIS Terra, western Queensland, Australia, J. Geophys. Res. Earth Surf., 113, 1–10, https://doi.org/10.1029/2007JF000765, 2008.

Nchaba, T., Mpholo, M., and Lennard, C.: Long-term austral summer wind speed trends over southern Africa, Int. J. Climatol., 37, 2850–2862, https://doi.org/10.1002/joc.4883, 2017.

Nield, J. M. and Baas, A. C. W.: The influence of different environmental and climatic conditions on vegetated aeolian dune landscape development and response, Glob. Planet. Change, 64, 76–92, https://doi.org/10.1016/j.gloplacha.2008.10.002, 2008.

Nield, J. M., Wiggs, G. F. S., and Squirrell, R. S.: Aeolian sand strip mobility and protodune development on a drying beach: Examining surface moisture and surface roughness patterns measured by terrestrial laser scanning, Earth Surf. Process. Landforms, 36, 513–522, https://doi.org/10.1002/esp.2071, 2011.

Okin, G. S., Bullard, J. E., Reynolds, R. L., Ballantine, J. A. C., Schepanski, K., Todd, M. C., Belnap, J., Baddock, M. C., Gill, T. E., and Miller, M. E.: Dust: Small-scale

892 processes with global consequences, Eos (Washington. DC)., 92, 241–242,
893 https://doi.org/10.1029/2011EO290001, 2011.
894 Palmer, B., Hernandez, R., and Lipson, D.: The fate of biological soil crusts after fire:
895 A meta-analysis, Glob. Ecol. Conserv., 24, e01380,
896 https://doi.org/10.1016/j.gecco.2020.e01380, 2020.
897 Parajuli, S. P. and Zender, C. S.: Connecting geomorphology to dust emission
898 through high-resolution mapping of global land cover and sediment supply, Aeolian
899 Res., 27, 47–65, https://doi.org/10.1016/j.aeolia.2017.06.002, 2017.
900 Planet Team: Planet Application Program Interface: In Space for Life on Earth, 2023.
901 Prospero, J. M., Ginoux, P., Torres, O., Nicholson, S. E., and Gill, T. E.:
902 Environmental characterization of global sources of atmospheric soil dust identified
903 with the Nimbus 7 Total Ozone Mapping Spectrometer (TOMS) absorbing aerosol
904 product, Rev. Geophys., 40, 2-1-2–31, https://doi.org/10.1029/2000RG000095, 2002.
905 Pye, K.: Processes of Fine Particle Formation, Dust Source Regions, and Climatic
906 Changes, in: Paleoclimatology and Paleometeorology: Modern and Past Patterns of
907 Global Atmospheric Transport, 3–30, https://doi.org/10.1007/978-94-009-0995-3_1,
908 1989.
909 Ravi, S., D'Odorico, P., Herbert, B., Zobeck, T., and Over, T. M.: Enhancement of
910 wind erosion by fire-induced water repellency, Water Resour. Res., 42, 1–9, https://
911 doi.org/10.1029/2006WR004895, 2006.
912 Ravi, S., D'Odorico, P., Zobeck, T. M., Over, T. M., and Collins, S. L.: Feedbacks
913 between fires and wind erosion in heterogeneous arid lands, J. Geophys. Res., 112,
914 G04007, 2007.
915 Reynolds, R. L., Yount, J. C., Reheis, M., Goldstein, H., Chavez, P., Fulton, R.,

916 Whitney, J., Fuller, C., and Forester, R. M.: Dust emission from wet and dry playas in
917 the Mojave Desert, USA, Earth Surf. Process. Landforms, 32, 1811–1827,
918 https://doi.org/10.1002/esp.1515, 2007.
919 Rodríguez-Caballero, E., Stanelle, T., Egerer, S., Cheng, Y., Su, H., Canton, Y.,
920 Belnap, J., Andreae, M. O., Tegen, I., Reick, C. H., Pöschl, U., and Weber, B.: Global
921 cycling and climate effects of aeolian dust controlled by biological soil crusts, Nat.
922 Geosci., 15, 458–463, https://doi.org/10.1038/s41561-022-00942-1, 2022.
923 van Rooyen, N. and van Rooyen, M. W.: Vegetation of the south-western arid
924 kalahari: An overview, Trans. R. Soc. South Africa, 53, 113–140,
925 https://doi.org/10.1080/00359199809520381, 1998.
926 Sankey, J. B., Eitel, J. U. H., Glenn, N. F., Germino, M. J., and Vierling, L. A.:
927 Quantifying relationships of burning, roughness, and potential dust emission with
928 laser altimetry of soil surfaces at submeter scales, 135, 181–190,
929 https://doi.org/10.1016/j.geomorph.2011.08.016, 2011.
930 Sankey, J. B., Germino, M. J., and Glenn, N. F.: Dust supply varies with sagebrush
931 microsites and time since burning in experimental erosion events, J. Geophys. Res.
932 Biogeosciences, 117, https://doi.org/10.1029/2011JG001724, 2012.
933 Schepanski, K.: Transport of mineral dust and its impact on climate, 8, 151,
934 https://doi.org/10.3390/geosciences8050151, 2018.
935 Stavi, I., Barkai, D., Knoll, Y. M., Glion, H. A., Katra, I., Brook, A., and Zaady, E.: Fire
936 impact on soil-water repellency and functioning of semi-arid croplands and
937 rangelands: Implications for prescribed burnings and wildfires, 280, 67–75,
938 https://doi.org/10.1016/j.geomorph.2016.12.015, 2017.
939 Suter-Burri, K., Gromke, C., Leonard, K. C., and Graf, F.: Spatial patterns of aeolian

sediment deposition in vegetation canopies: Observations from wind tunnel experiments using colored sand, Aeolian Res., 8, 65–73, https://doi.org/10.1016/j.aeolia.2012.11.002, 2013.

Sweeney, M. R. and Mason, J. A.: Mechanisms of dust emission from Pleistocene loess deposits, Nebraska, USA, J. Geophys. Res. Earth Surf., 118, 1460–1471, https://doi.org/10.1002/jgrf.20101, 2013.

Sweeney, M. R., McDonald, E. V., and Etyemezian, V.: Quantifying dust emissions from desert landforms, eastern Mojave Desert, USA, 135, 21–34, https://doi.org/10.1016/j.geomorph.2011.07.022, 2011.

Sweeney, M. R., Lu, H. Y., Cui, M. C., Mason, J. A., Feng, H., and Xu, Z. W.: Sand dunes as potential sources of dust in northern China, Sci. China Earth Sci., 59, 760–769, https://doi.org/10.1007/s11430-015-5246-8, 2016.

Sweeney, M. R., Lacey, T., and Forman, S. L.: The role of abrasion and resident fines in dust production from aeolian sands as measured by the Portable in situ Wind Erosion Laboratory (PI-SWERL), Aeolian Res., 63–65, 100889, https://doi.org/10.1016/j.aeolia.2023.100889, 2023.

Swet, N., Elperin, T., Kok, J. F., Martin, R. L., Yizhaq, H., and Katra, I.: Can active sands generate dust particles by wind-induced processes?, Earth Planet. Sci. Lett., 506, 371–380, https://doi.org/10.1016/j.epsl.2018.11.013, 2019.

Thomas, A. D. and Dougill, A. J.: Distribution and characteristics of cyanobacterial soil crusts in the Molopo Basin, South Africa, J. Arid Environ., 64, 270–283, https://doi.org/10.1016/j.jaridenv.2005.04.011, 2006.

Thomas, A. D. and Dougill, A. J.: Spatial and temporal distribution of cyanobacterial soil crusts in the Kalahari: Implications for soil surface properties, 85, 17–29, https://

964 doi.org/10.1016/j.geomorph.2006.03.029, 2007.
965 Thomas, D. S. G. and Leason, H. C.: Dunefield activity response to climate variability
966 in the southwest Kalahari, 64, 117–132,
967 https://doi.org/10.1016/j.geomorph.2004.06.004, 2005.
968 Urban, F. E., Goldstein, H. L., Fulton, R., and Reynolds, R. L.: Unseen Dust Emission
969 and Global Dust Abundance: Documenting Dust Emission from the Mojave Desert
970 (USA) by Daily Remote Camera Imagery and Wind-Erosion Measurements, J.
971 Geophys. Res. Atmos., 123, 8735–8753, https://doi.org/10.1029/2018JD028466, 2018.
972 Vos, H. C., Fister, W., Eckardt, F. D., Palmer, A. R., and Kuhn, N. J.: Physical crust
973 formation on sandy soils and their potential to reduce dust emissions from
974 croplands, 9, 1–20, https://doi.org/10.3390/land9120503, 2020.
975 Vos, H. C., Fister, W., von Holdt, J. R. C., Eckardt, F. D., Palmer, A. R., and Kuhn, N.
976 J.: Assessing the PM10 emission potential of sandy, dryland soils in South Africa
977 using the PI-SWERL, Aeolian Res., 53, 100747,
978 https://doi.org/10.1016/j.aeolia.2021.100747, 2021.
979 Wagenbrenner, N. S., Chung, S. H., and Lamb, B. K.: A large source of dust missing
980 in particulate matter emission inventories? Wind erosion of post-fire landscapes, 5,
981 https://doi.org/10.1525/elementa.185, 2017.
982 Walker, I. J., Hilgendorf, Z., Gillies, J. A., Turner, C. M., Furtak-Cole, E., and
983 Nikolich, G.: Assessing performance of a “nature-based” foredune restoration
984 project, Oceano Dunes, California, USA, Earth Surf. Process. Landforms, 48, 143–162,
985 https://doi.org/10.1002/esp.5478, 2023.
986 Wang, Y., Yan, P., Wang, Y., Wang, X., Wu, W., and Dong, M.: Dust emission from
987 different land use types based on the PI-SWERL test, 248, 108577,

https://doi.org/10.1016/j.catena.2024.108577, 2025.

Wasson, R. J. and Nanninga, P. M.: Estimating wind transport of sand on vegetated surfaces, Earth Surf. Process. Landforms, 11, 505–514, https://doi.org/10.1002/esp.3290110505, 1986.

Webb, N. P. and Strong, C. L.: Soil erodibility dynamics and its representation for wind erosion and dust emission models, Aeolian Res., 3, 165–179, https://doi.org/10.1016/j.aeolia.2011.03.002, 2011.

Webb, N. P., McCord, S. E., Edwards, B. L., Herrick, J. E., Kachergis, E., Okin, G. S., and Van Zee, J. W.: Vegetation Canopy Gap Size and Height: Critical Indicators for Wind Erosion Monitoring and Management, Rangel. Ecol. Manag., 76, 78–83, https://doi.org/10.1016/j.rama.2021.02.003, 2021.

Weber, B., Belnap, J., Büdel, B., Antoninka, A. J., Barger, N. N., Chaudhary, V. B., Darrouzet-Nardi, A., Eldridge, D. J., Faist, A. M., Ferrenberg, S., Havrilla, C. A., Huber-Sannwald, E., Malam Issa, O., Maestre, F. T., Reed, S. C., Rodríguez-Caballero, E., Tucker, C., Young, K. E., Zhang, Y., Zhao, Y., Zhou, X., and Bowker, M. A.: What is a biocrust? A refined, contemporary definition for a broadening research community, Biol. Rev., 97, 1768–1785, https://doi.org/10.1111/brv.12862, 2022.

Wiggs, G. F. S., Livingstone, I., Thomas, D. S. G., and Bullard, J. E.: Effect of vegetation removal on airflow patterns and dune dynamics in the southwest Kalahari desert, L. Degrad. Dev., 5, 13–24, https://doi.org/10.1002/ldr.3400050103, 1994.

Wiggs, G. F. S., Thomas, D. S. G., and Bullard, J. E.: Dune Mobility and vegetation cover in the southwest Kalahari Desert, Earth Surf. Process. Landforms, 20, 515–529, 1995.

Wiggs, G. F. S., Baddock, M. C., Thomas, D. S. G., Washington, R., Nield, J. M., Engelstaedter, S., Bryant, R. G., Eckardt, F. D., von Holdt, J. R. C., and Kötting, S.: Quantifying Mechanisms of Aeolian Dust Emission: Field Measurements at Etosha Pan, Namibia, J. Geophys. Res. Earth Surf., 127, 1–21, https://doi.org/10.1029/2022JF006675, 2022.

Yu, Y. and Ginoux, P.: Enhanced dust emission following large wildfires due to vegetation disturbance, Nat. Geosci., 15, 878–884, https://doi.org/10.1038/s41561-022-01046-6, 2022.